Chinese Journal of Oceanology and Limnology
Vol. 29 No. 2, P. 446-459, 2011
DOI: 10.1007/s00343-011-0114-7

A spectral mixture model analysis of the Kuroshio variability and the water exchange between the Kuroshio and the East China Sea*

SONG Jun (宋军)[1, 2, 3], XUE Huijie (薛惠洁)[2], BAO Xianwen (鲍献文)[1, **],
WU Dexing (吴德星)[1, **], CHAI Fei (柴扉)[2], SHI Lei (施磊)[2], YAO Zhigang (姚志刚)[1],
WANG Yongzhi (王勇智)[4], NAN Feng (南峰)[1], WAN Kai (万凯)[1]

[1] *Physical Oceanography Laboratory, Ocean University of China, Qingdao 266100, China*

[2] *School of Marine Sciences, University of Maine, Orono, ME 04469, United States*

[3] *National Marine Data and Information Service, Tianjin 300171, China*

[4] *The First Institute of Oceanography, SOA, Qingdao 266061, China*

Received Apr. 9, 2010; revision accepted Oct. 10, 2010

Abstract For understanding more about the water exchange between the Kuroshio and the East China Sea, We studied the variability of the Kuroshio in the East China Sea (ECS) in the period of 1991 to 2008 using a three-dimensional circulation model, and calculated Kuroshio onshore volume transport in the ECS at the minimum of 0.48 Sv (1 Sv $\equiv 10^6$ m^3/s) in summer and the maximum of 1.69 Sv in winter. Based on the data of WOA05 and NCEP, The modeled result indicates that the Kuroshio transport east of Taiwan Island decreased since 2000. Lateral movements tended to be stronger at two ends of the Kuroshio in the ECS than that of the middle segment. In addition, we applied a spectral mixture model (SMM) to determine the exchange zone between the Kuroshio and the shelf water of the ECS. The result reveals a significantly negative correlation (coefficient of -0.78) between the area of exchange zone and the Kuroshio onshore transport at 200 m isobath in the ECS. This conclusion brings a new view for the water exchange between the Kuroshio and the East China Sea. Additional to annual and semi-annual signals, intra-seasonal signal of probably the Pacific origin may trigger the events of Kuroshio intrusion and exchange in the ECS.

Keyword: East China Sea (ECS); Kuroshio; spectral clustering; spectral mixture model; water mass analysis; water exchange

1 INTRODUCTION

The East China Sea (ECS) is a large marginal sea in the western Pacific, which has the world's vastest continental shelf. Out of a total area of 1.25×10^6 km^2, the shelf region (depth $<$200 m) amounts to 0.9×10^6 km^2 (Wang et al., 2000; Lin et al., 2002; Hu et al., 2007). The Kuroshio, the western boundary current in the western north Pacific, originates from the North Equatorial Current (NEC) that bifurcates off the Philippine coast (Nitani, 1972; Guo et al., 2003). The Kuroshio, after sometimes looping into the South China Sea via the Luzon Strait sometimes, flows by east of Taiwan Island and then in a northeastward direction along the continental slope in the ECS (Nitani, 1972; Guo et al., 2003; Andres et al., 2008). The Kuroshio determines the mass transport of the subtropical gyre in the Pacific, and consequently exerts strong influences on the regional climate (Guo et al., 2003; Ma et al., 2009). It also affects the complicated seasonal circulation and interannual variability of the currents in the ECS (Mizuno et al., 1983; Yanagi et al., 1993; Bao et al., 2005).

* Supported by the National Basic Research Program of China (973 Program) (Nos. 2005CB422300, 2007CB411804, 2010CB428904), the National Natural Science Foundation of China (Nos. 40976001, 40940025, 41006002), Tianjin Municipal Science and Technology Commission Project (No. 09JCYBJC07400), the "111 Project" (No. B07036), and the Program for New Century Excellent Talents in University (No. NECT-07-0781)

** Corresponding author: xwbao@ouc.edu.cn; dxwu@ouc.edu.cn

To understand the Kuroshio variability and the interplay between the ECS shelf water and the water brought by the Kuroshio, many valuable studies have been carried out in the past decades (Guan, 1980; Wong et al., 2000; Johns et al., 2001; Teague et al., 2003; Guo et al., 2003 and 2006; Lee et al, 2007; Ma et al., 2009). The core position of the Kuroshio and its variability have been studied extensively. Estimated transport across key sections in the ECS and the associated variability from some of the previous studies are summarized in Table 1. Using the observations from moored current meters and Acoustic Doppler Current Profilers (ADCPs) between September 1994 and May 1996, Johns et al. (2001) estimated the mean Kuroshio transport at 21.5 Sv east of Taiwan Island. The decrease in Kuroshio transport during the 1997 El Nino was observed by Yuan et al. (2001). Based on the observations collected in October–December, 1999, Teague et al. (2003) calculated the volume, heat and salt transports in the ECS and concluded that the volume transport through the Taiwan Strait and Tsushima Strait were 0.14 and 3.17 Sv, respective. Similarly, Lin et al. (2005) estimated the fall/winter transport through the Taiwan Strait at 0.12±0.33 Sv. Using a 1/18 deg nested ocean model, Guo et al. (2003 and 2006) analyzed the current and volume transport in the ECS. The mean volume transport through the Taiwan Strait was 1.71 Sv, which was much larger than the fall/winter estimate of Teague et al. (2003) and Lin et al. (2005).

With the advancement of observational means and numerical models, several comprehensive studies further analyzed the interaction between the Kuroshio and the shelf water in recent years. Guo et al. (2006) calculated the seasonal variation of the Kuroshio onshore flux across the 200 m isobath in the ECS, which reached the maximum around 2 Sv in autumn and the minimum less than 0.5 Sv in summer. They also suggested that the Ekman transport due to wind stress influences prominently the seasonal variability of this onshore transport. The model of Lee and Matsuno (2007) estimated the transport across the 200 m isobath at 2.74 Sv in winter and 2.47 Sv in summer, which was heavily influenced by the variations of the transport through the Taiwan Strait and that east of Taiwan Island. Matsuno et al. (2009) revealed that the Kuroshio intrusion into the shelf region of the ECS has distinct seasonal variation and the Taiwan Warm Current plays a significant role in determining the Kuroshio intrusion. They further concluded that the bottom topography, wind stress, vertical mixing and frontal eddies are important factors that influence the water exchange between the Kuroshio and the shelf water in the ECS. Using the Argos drifter buoy data and TOPEX/Poseidon altimeter data, the structure and variability of the surface velocity in the ECS was studied by Ma et al. (2009). Their result showed that different segments of the Kuroshio are controlled by the variability of different dominant periods. Some of those periods should originate from the westward propagating Rossby Waves (Wei et al., 2004) or the Kuroshio frontal instability (Jia et al., 2005).

Other researches focused on the region east and northeast of Taiwan Island (Chern et al., 1990; Tang and Yang, 1993; James et al., 1999; Morimoto et al., 2009). The Kuroshio Edge Exchange Processes (KEEP) studied the material exchange between the ECS and the Kuroshio

Table 1 The ROMS estimated net transports at key cross-sections in the ECS (TS) in comparison with the transport specified by Lee and Matsuno (2007) and the annual mean estimates of Guo et al. (2006) and Teague et al. (2003). Other values include the 20-month average near 24°N at 21.5 Sv (Johns et al., 2001); annual mean transport across the 200 m isobath at 0.85 Sv (Isobe, 2006) and 1.4 Sv (Isobe, 2008). In addition, Guo et al. (2006) also showed that the transport across the 200 m isobath is <0.5 Sv in summer and ~ 3 Sv in fall

Flux(Sv) (1 Sv≡10^6 m^3/s)	Spring TS/LM	Summer TS/LM	Fall TS/LM (Teague et al., 2003)	Winter TS/LM	Annual Mean TS (Guo et al., 2006)
Section 24°N	25.3/21	25.9/24	24.9/20/23	24.6/22	25.1/23.83
Section 130°E	22.2/20	23.7/24	22.7/18/20.0	21.2/21	22.4/19.47
Taiwan Strait	1.6/1.5	2.6/2.5	1.7/1.5/0.14	1.0/0.9	1.7/1.71
Tsushima Strait	2.6/2.3	3.2/2.7	3.6/3.0/3.17	3.0/2.1	3.1/3.03
200 m isobath	0.95/2.43	0.48/2.47	1.63/2.84/3.0	1.69/2.74	1.18/1.46

(Wong, et al., 2000). Chern et al. (1990) and James et al. (1999) suggested that the Kuroshio frontal variability and the associated filaments and cold eddies were a major factor that induces exchanges between the ECS shelf water and the Kuroshio water. Tang and Yang (1993) observed the intrusion of the Kuroshio onto the shelf region northeast of Taiwan Island, which has a weak relationship with the local wind. On the other hand, Chuang and Liang (1994) suggested that cold air outbreaks may be the major cause for triggering Kuroshio intrusions northeast of Taiwan Island in winter. In addition, short-period intrusions induced by typhoons were observed by Chuang and Liang (1994) and Morimoto et al. (2009).

There have also been numerous studies that considered the exchange processes between the Kuroshio water and the shelf water in the ECS based on water mass analyses and isotope tracer experiments (Chen et al., 1995; Kim et al., 2005; Jan et al., 2006; Li et al., 2006; Zuo et al., 2006; Takikawa et al., 2008; Lan et al., 2009). For example, using the oxygen isotopes, Kim et al. (2005) revealed that the Tsushima Current has two water sources: waters from the Taiwan Strait and the Kuroshio. These articles add a heuristic view for studying the circulation in the ECS.

The previous studies often described the exchange between the Kuroshio water and the ECS shelf water using the fluxes across the shelf break. This definition doesn't clearly distinguish between the Kuroshio lateral movement and the exchange processes as the onshore flux of the Kuroshio may exit from the Tsushima Strait without participating in the exchange processes. A more clear definition would be arguably based on water mass analyses. In this study, the Spectral Mixture Model is applied to the temperature and salinity fields obtained from a Pacific basin-wide model simulation from 1991 to 2008 to determine the exchange zone between the Kuroshio and the shelf water in ECS. The Pacific basin-wide model is introduced in Section 2. The model simulated Kuroshio and its variability are also discussed in this section. The Spectral Mixture Model, which has been widely used in graph theory in computer sciences along with the adaption implemented for this study is described in Section 3. The relationship between the variability of the exchange zone and the Kuroshio onshore flux in the ECS is then discussed in Section 4.

2 MODEL AND RESULT

2.1 Model configuration

The 3-D circulation model used in this study is based on the Regional Ocean Model System (ROMS). ROMS is a free-surface, hydrostatic, primitive equation ocean model that uses stretched, terrain-following coordinates in the vertical and orthogonal curvilinear coordinates in the horizontal (Shchepetkin et al., 1998; 2003; 2005). The vertical mixing in the bottom and surface boundary layers uses the K-profile parameterization of Large et al. (1994). In this application, the ROMS has been configured for the Pacific Ocean from 45°S to 65°N and 99°E to 70°W at 12.5 km resolution. There are 30 s-levels in the vertical.

The initial condition and boundary condition for temperature and salinity field are derived from the World Ocean Atlas (WOA) 2005 (http://www.nodc.noaa.gov/OC5/WOA05/pr_woa05.html). The surface forcing data include wind stress, shortwave radiation, longwave radiation, sensible and latent heat fluxes, precipitation and evaporation, except the wind all of which are derived from the $2° \times 2°$ resolution daily product from the National Center for Environmental Prediction (http://nomads.ncep.noaa.gov/txt_descriptions/servers.shtml). The daily $1/4° \times 1/4°$ resolution sea surface wind stress is obtained from the Blended Sea Winds (ftp://eclipse.ncdc.noaa.gov/raid1b/seawinds/SI/). Note that the present simulation doesn't include rivers or tides as the model was originally developed for the general circulation and the biogeochemistry in the Pacific Ocean. Nevertheless, it has been shown that the marginal seas in the western Pacific are reasonably simulated especially in terms of long term trends. Results from the same model and its predecessor at 50 km resolution have been used to examine eddy activities (Xiu et al., 2010) and biogeochemical processes in the South China Sea (Chai et al., 2009; Liu and Chai, 2009). This study uses the monthly averaged model results for the period from 1991 to 2008, and our analysis focuses on the Kuroshio and the ECS in the area from 24° to 35°N and from 118° to 130°E (Fig.1).

2.2 The modeled Kuroshio and its seasonal variability

The modeled velocity field at 5 m depth is averaged for the period from 1991 to 2008, which

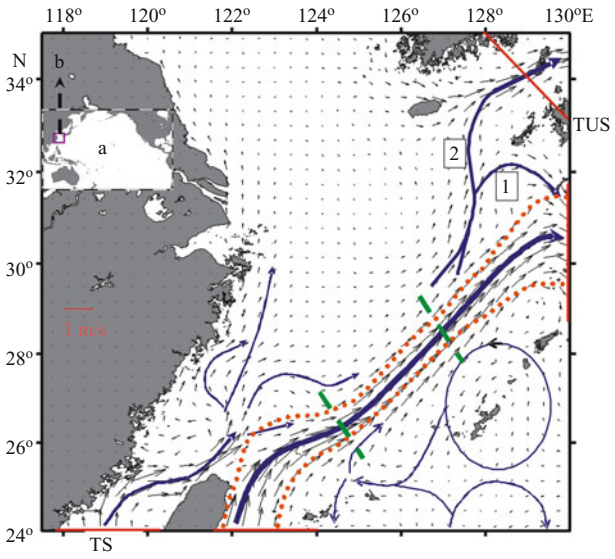

Fig.1 (a) The Pacific ROMS model domain and (b) the focal region of this study

The 5 m mean velocity field is shown as the black arrows, one arrow of every four grids only. The blue curved arrows show the schematic annual mean surface currents in the East China Sea (ECS). The zone between the two orange dashed lines shows the range of the Kuroshio axis during the 18-year simulation. The two green dashed lines divide the Kuroshio to three segments, the southwestern segment, the mid segment and the northeastern segment from left to right. Several key cross-sections are shown in red lines: TS: Taiwan Strait; 24°N: Kuroshio east of Taiwan at 24°N; 130°E: Kuroshio in the Tokara Strait at 130°E; and TUS: Tsushima Strait

is shown in Fig.1. The Kuroshio as the intense western boundary current in the north Pacific is successfully modeled. The simulated Kuroshio flows from east of Taiwan Island northeastward along the continental and exits the study area through the Tokara Strait. Several currents in the ECS shelf are directly related to the Kuroshio. For example, the northward current in the Taiwan Strait comes partly from the Kuroshio intrusion into the South China Sea (Fig.2, Spring) and partly from the South China Sea coastal current (Fig.2, Summer). Immediately northeast of the Taiwan Island, the shelf side of the Kuroshio often peels off to loop anticyclonically onto the shelf, which joins the warm current emerging from the Taiwan Strait and fans out as several northwest-, north-, and northeastward currents in the southern ECS shelf. At about 30°N, the shoreward side of the Kuroshio peels off again to flow northward along the shelfbreak (marked as the Current 2 in Fig.1), which later becomes the main source for the Tsushima Current to enter the Sea of Japan. In addition, a branch separates from Current 2 southwest of Kyushu. The branch (designated as Current 1) curves anticyclonically to merge again with the Kuroshio in the Tokara Strait.

Fig.1 shows the Kuroshio as a strong western boundary current east of the Taiwan Island (Stommel, 1948; Fukuoka, 1957). Meanwhile, based on the Bernoulli Principle (Batchelor, 1967; Clancy, 1975), a decrease in the potential energy or pressure of the Kuroshio should accompany the occurrence of an increase in the speed of the Kuroshio. This sudden change, which brings the negative vorticity, cannot be balanced by the Coriolis Force, so that the Kuroshio flows close to the east coast of the Taiwan Island and is adjusted to an equilibrium state by increasing the frictional force, which generates the positive vorticity. Based on the theory of Island Integral Constraint, this friction force may be a mechanism for steering the flow into the Taiwan Strait (Yang, 2007).

The seasonal variation shown in Fig.2 suggests that the modeled Kuroshio is the strongest in spring and summer but becomes weaker in fall and winter. This agrees with the finding of Zhou et al. (2006). As explained by Guo et al. (2006), the seasonal variability is mostly wind-driven with the density effect playing the secondary role. To describe different behaviors of the Kuroshio, we divide the current into three segments based on the degree of the lateral movements (the two orange dashed lines in Fig.1). They are designated as the southwestern segment, the mid segment, and the northeastern segment from the left to the right.

The Kuroshio axis moves from side to side around its mean position, and the two end segments experience more frequent and greater extent lateral movements compared to the mid segment. For the southwestern segment, the position of the Kuroshio axis is further to the east in spring and summer than in fall and winter (Fig.2). This appears to be related to the decline of the northward current from the Taiwan Strait (Fig.2 Fall and Winter) due to the winter monsoon as explained by Hsueh et al. (1993). The Kuroshio position is also known to respond to extreme weathers. For example, the Kuroshio was observed to move onto the shelf northeast of Taiwan Island as Typhoon Hai-Tang passed by the area from 11 to 21 July 2005 (Morimoto et al., 2009). The Kuroshio in the mid segment has the most stable path among all three segments as seen in Fig.1. We speculate that this area facilitates a wide range of the frictional force to stabilize the Kuroshio. The northeastern segment exhibits most seasonal changes. In this segment, Current

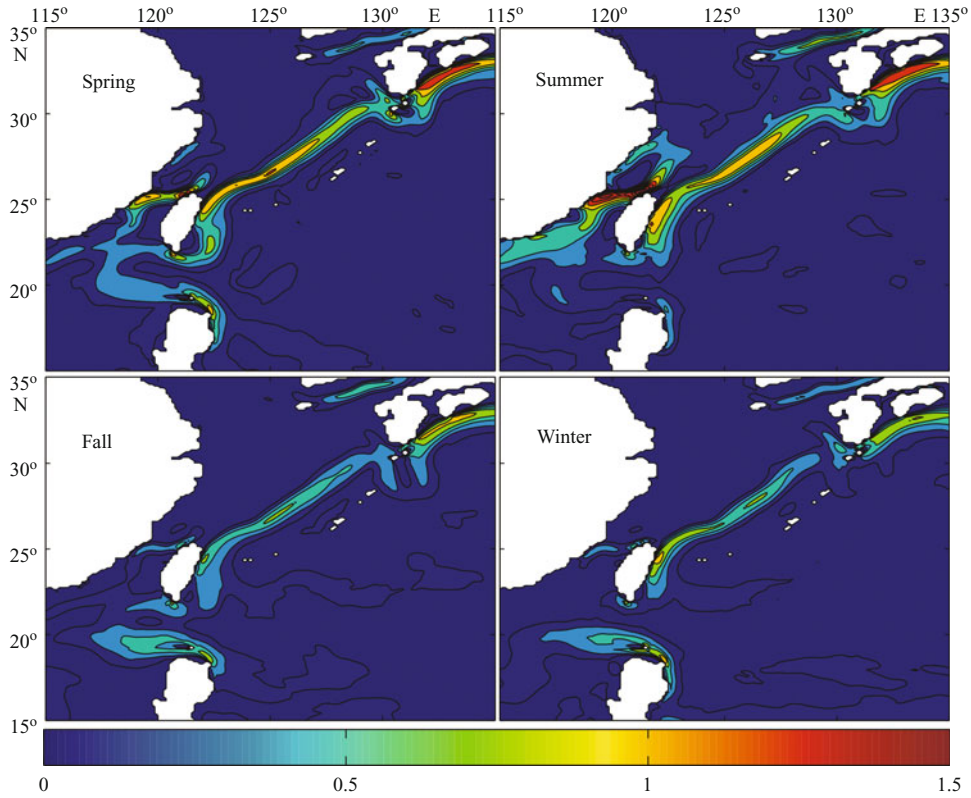

Fig.2 The seasonally averaged, surface speed from the model, showing clearly the area of strong currents including the Kuroshio, the Tsushima Current, and the currents in the Taiwan Strait (unit: m/s)

1 is strongest in spring and weakest in fall. It has a complementary relationship with the Kuroshio. Current 2, which is a main source of the Tsushima Current, reaches the greatest strength in summer but weakest in winter.

2.3 Transport across the Section TS, TUS, 24°N, 130°E and the 200 m isobath

We calculated the transport across five representative sections (see the red lines in Fig.1 and the red curve in Fig.4). Wide cross-sections are used to calculate the transport at 24°N and 130°E. Following Chen et al. (2006) the speed contour of 15 cm/s is used as the bound in calculating the Kuroshio transport along with the 1 000 m depth limit in the vertical. The annual mean and seasonal transport derived from the 18 year simulation are given in Table 1. The annual mean values compare favorably with the estimates of Guo et al. (2006) with slightly higher transport at both 24°N and 130°E. On the other hand, the seasonal tendency agrees with that specified by Lee and Matsuno (2007) for the Taiwan Strait and the Tsushima Strait, but disagrees for the 24°N and 130°E sections. The ROMS Pacific simulation shows the maximum transport of the Kuroshio in summer and the minimum in winter both at 24°N and 130°E, whereas according to Lee and Matsuno (2007) the minimum occurs in October. However, Lee and Matsuno's estimates were derived from the sea-level difference time series.

Time series of the monthly transport through these sections from 1991 to 2008 (Fig.3) show a generally positive correlation between the Kuroshio flux at 24°N and that at 130°E. The changes of flux at 24°N is often earlier than the flux at 130°E but sometimes later as in 1997 and 2004. It is therefore hard to conclude that the Kuroshio variability upstream could totally control the variability downstream in the ECS. In the model seasonal variability of the transport at 24°N becomes small after 2000. This, however, does not seem to affect the seasonal variability at 130°E.

The transport through the Taiwan Strait (TS) and the Tsushima Strait (TUS) (Fig.3b) and the transport across the 200 m isobath (Fig.3c) define the water budget in the ECS and Yellow Sea. The TS transport has a highly positive correlation with the TUS transport with the latter having a 3-month delay, suggesting the TS transport is a factor that influences the exiting flux through the

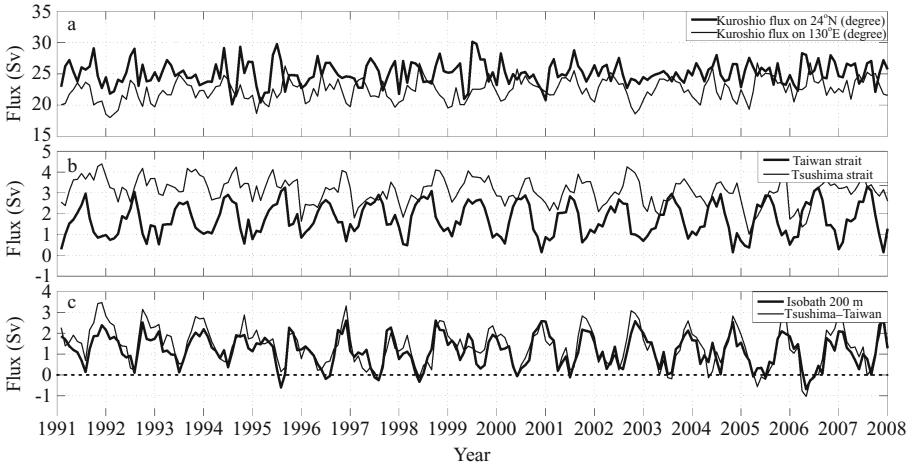

Fig.3 Monthly volume transports from 1991 to 2008

a. Volume transports at 24°N (the thick line) and 130°E (the thin line); b. Volume transports through the TS (the thick line) and the TUS (the thin line); c. Onshore transport across the 200-m isobath (the thick line) and the difference between the volume through the TS and that through the TUS (the thin line). Positive values represent northward (24°N section, TS), eastward (130°E section), northeastward (TSU) and onshore (200-m isobath) fluxes

TUS. On the other hand, the TUS transport is almost twice the TS transport, implying that waters of different origins also contribute to the TUS transport. The net transport across the 200 m isobath appears to close the budget with the time series closely following the difference between the TUS transport and the TS transport (Fig.3c). On the average, the net transport across the 200 m isobath on to the shelf has a well-defined annual cycle with it being the highest (~2 Sv) in September–November and gradually decreasing to a minimum (~1.3 Sv) in June and July the following year.

Fluxes across the 200 m isobath, which is a popular index for representing the exchange between the Kuroshio and shelf waters in the ECS, is further analyzed. Fig.4 shows the climatological mean distribution of the flux along the 200 m isobath. Also plotted are reporting positions from 31 Argo profiling floats in the Northwest Pacific (24°–36°N, 117°–130°E). A total of 3 258 registered float positions are shown in Fig.4 for all the years from 2003 to 2007, a11 of which are provided by the China Argo Real-time Data Center (ftp://www.argo.gov.cn/). To ensure the accuracy and reliability of these data, both the real-time and delayed-mode quality control were made (Tong et al., 2003). The Argo data are not sufficient for calculating the flux, but their positions are shown as a reference to indicate possible advection onto the shelf.

The interleaving distribution of the fluxes across the 200 m isobath would suggest the presence of mesoscale features. Influenced by the Kuroshio, the magnitudes of the fluxes are larger and on the average onto the shelf in the southwestern and mid segment. The northeastern segment deviates from the main axis of the Kuroshio. The magnitudes of the fluxes there are usually smaller than those in the first two segments, and the net transport for the northeastern segment is almost nil. Similar result was also shown by Guo et al. (2006) and the

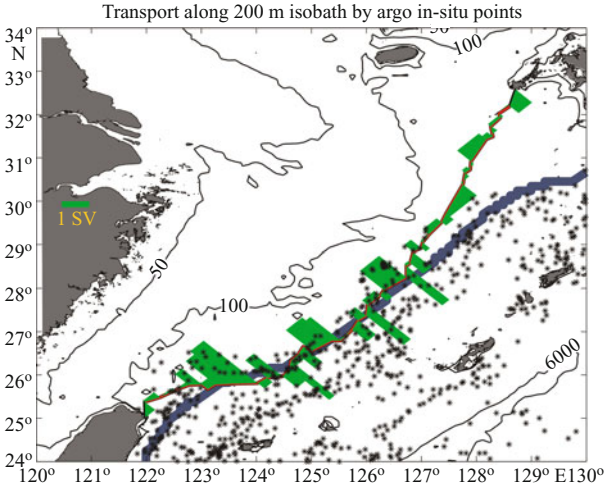

Fig.4 The axis of the Kuroshio, shown as the heavy blue line, is derived as the location of the maximum surface flow speed from the mean of the 18-year simulation

The thin red line shows the 200-m isobath in the ECS, which is the location where we calculate the flux of the Kuroshio water onto the continental shelf. The length of the green bars indicates the magnitude of the annual mean fluxes across the 200-m isobath. The black asterisks are the reporting locations of Argo buoys at different times in the period from 2003 to 2007

strong correlations among the variability of these three transports were also reported by Lee and Matsuno (2007).

3 THE SPECTRAL MIXTURE MODEL

The model result shows clearly that the fluxes onto the ECS shelf is strong in fall and early winter (Fig.3) and weak in summer and that the onshore fluxes across the shelfbreak is highest north of Taiwan Island in the southern ECS (Fig.4). This is most likely related to that the mean position of the Kuroshio is more onto the shelf (away from the mean Kuroshio axis seen in Fig.1) in winter than in summer. The questions is to what degree the onshore fluxes represent the exchange of the Kuroshio water and the shelf water rather than the inflow of the Kuroshio water that subsequently exits from the TUS. An alternative definition that can better represent the exchange is needed.

T-S diagram has been a standard tool in water mass analysis since its application by Sverdrup et al. (1942). For example, it was used by Miller (1950) to study water mass divisions. In recent years, the methods of membership function (Li et al., 2004) and cluster analysis (Su et al., 1983) were adopted to analyze the mixed water masses. However, the method of membership function tailors the prespecified T-S curve shapes and often needs many adjustments when applied to different regions. The classic cluster analysis can be used more generally, but it sometimes fails to catch principal directions especially when the T-S distributions appear to be widely scattered. Moreover, both methods are inefficient in processing massive datasets.

Base on recent developments of graph theory in mathematics, the Spectral Mixture Model (SMM) is adapted to define an exchange belt between the Kuroshio water and the shelf water and to investigate its variability using the modeled temperature and salinity. To our knowledge, the method is being used in oceanographic applications for the first time, and hereby it is described in details below.

3.1 Algorithm

For clarity, we define a set, $\boldsymbol{P} = \{P_1, \ldots, P_n\}$, to represent all object points in the study domain, where n is the number of all points. The set $\boldsymbol{M} = \{m_1, \ldots, m_k\}$ is defined to represent all possible clusters, which divides the set $\boldsymbol{P}$. The total number of the clusters, k, should be less than n. The SMM consists of three steps. First of all, the set of object points is divided into any number of clusters using the spectral clustering method. The number of clusters and the associated centroids are determined in this step. Secondly, the probability of each $m_i \subset \boldsymbol{M}$ from the first step by all $P_j \in \boldsymbol{P}$ is calculated. Lastly, an exchange zone is defined for any two clusters that belong to $\boldsymbol{M}$. Different from classic mixture models, SMM determines the principal distribution direction using spectral clustering. Moreover, this method also considers the influence sphere of each cluster while calculating the probability density functions. The influence sphere of a cluster is a spherical space that encompasses all points of the cluster.

3.1.1 Spectral clustering

Spectral Clustering (SC) is one of the most popular modern clustering algorithms developed in the beginning of the 21st century (Ulrike, 2007). SC is based on graph theory. It has been wildly used in Computer Sciences, such as artificial vision systems (Jitendra et al., 2001), machine learning (Shi, 2000) and other subjects in biochemistry (Menschaert et al., 2009). As it considers not only the difference among all the object points, but also the connectivity as a whole, SC appears to be superior in computational efficiency (Ng et al., 2002) and in getting a global optimum especially in convex regions (Luo et al., 2003). In brief, SC considers each $P_i \in \boldsymbol{P}$ as a vertex in the graph G (Fig.5). G is an undirected but weighted graph with a positive semi-definite, symmetric weighting

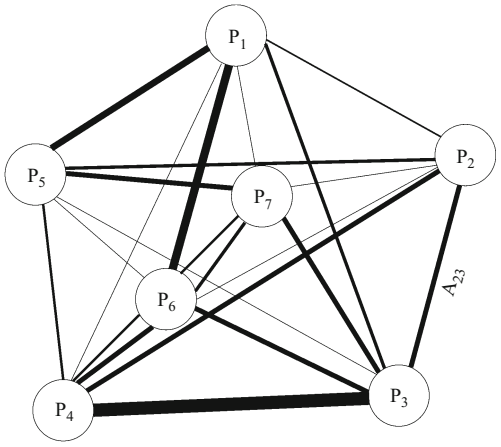

Fig.5 Similarity graph G ($\boldsymbol{P}$, $\boldsymbol{A}$)

The edge weight (represented by the width in this graph) of A indicates the similarity between two vertex points. For example, A_{23} as the edge weight for vertexes P_2 and P_3. In this study, the vertices represent the water properties from every model grid points

matrix $\boldsymbol{A}$ ($A_{ij}=A_{ji}\geq 0$) that represents the similarity between P_i and P_j. A_{ij} is commonly expressed as the distance that separates P_i and P_j in the parameter space. In graph G ($\boldsymbol{P}$, $\boldsymbol{A}$), solving the clustering problem is equivalent to minimizing the graph cut.

To help define the cut, the notation $A(\boldsymbol{M}, \boldsymbol{N}) := \sum_{i\in \boldsymbol{M}, j\in \boldsymbol{N}} A_{ij}$ is introduced, where $\boldsymbol{M}$ and $\boldsymbol{N}$ are any two clusters. We also introduce $\overline{\boldsymbol{m}_i}$ as the complement of $\boldsymbol{m}_i$. The graph cut is then defined as the following:

$$cut\ (\boldsymbol{m}_1,\ldots,\boldsymbol{m}_k) := \frac{1}{2}\sum_{i=1}^{k} A(\boldsymbol{m}_i,\overline{\boldsymbol{m}_i}) \tag{1}$$

To avoid having any single vertex be separated from the rest of the graph, in many cases like ours, an updated definition for cut known as the normalized cut (Ncut) is used.

$$\text{Ncut}\ (\boldsymbol{m}_1,\ldots,\boldsymbol{m}_k) := \frac{1}{2}\sum_{i=1}^{k} \frac{A(\boldsymbol{m}_i,\overline{\boldsymbol{m}_i})}{vol(\boldsymbol{m}_i)} \tag{2}$$

where $vol(\boldsymbol{m}_i)=\sum_{i\in \boldsymbol{m}_i} A_{ij}$. To minimize Ncut, the SC algorithm is the most direct way (von, 2007). For the set of points $\boldsymbol{P}$ in $\mathbb{R}^1$ ($\mathbb{R}$ represents the set of all real numbers, the superscript indicates the dimensions of $\mathbb{R}$), which will be divided into k clusters, the entire SC algorithm is simply described below.

1) Construct an affinity matrix $\boldsymbol{A}\in\mathbb{R}^{n\times n}$. In this study we use the Gaussian similarity function to define A.

$$A_{ij}=\exp\left(-\left\|p_i-p_j\right\|^2\Big/\left(2\sigma^2\right)\right) \tag{3}$$

The scaling parameter, σ, determines the decline rate of A_{ij} given the distance between p_i and p_j. Although there are methods for optimizing σ automatically (von, 2007), it is simply set to 1 in this case because all data had been standardized.

2) Define a diagonal matrix $\boldsymbol{D}$ with D_{ii} being the sum of all values in the i^{th} row of $\boldsymbol{A}$:

$$D_{ii}=\sum_{j=1}^{n} A_{ij} \tag{4}$$

3) Define a Laplacian matrix $\boldsymbol{L}$, a positive semi-definite matrix:

$$\boldsymbol{L}=\boldsymbol{D}^{-1/2}\boldsymbol{A}\boldsymbol{D}^{-1/2} \tag{5}$$

4) Obtain the k smallest eigenvalues (λ_1,…, λ_k) and their corresponding eigenvectors ($\overrightarrow{x_1}$,…, $\overrightarrow{x_k}$) of $\boldsymbol{L}$;

5) Let the object matrix $\boldsymbol{O}=(\overrightarrow{(x)}_1,\ldots,\overrightarrow{(x)}_k)\in\mathbb{R}^{n\times k}$ be the matrix stacking the eigenvectors in columns.

6) Form the matrix $\boldsymbol{Q}\in\mathbb{R}^{n\times k}$ from $\boldsymbol{O}$ by normalizing each row of $\boldsymbol{O}$ to have unit length.

$$\boldsymbol{Q}_{ij}=\frac{\boldsymbol{O}_{ij}}{(\sum_j \boldsymbol{O}_{ij}^2)^{1/2}} \tag{6}$$

7) Treat each row of $\boldsymbol{Q}$ as a point in P. This means $\boldsymbol{Q}$ could be seen as an array of N points by k attributes. Divide them into clusters of $\boldsymbol{M}$ using the K-means algorithm or any other traditional clustering algorithm. Meanwhile, the centroid associated with each cluster is determined.

The K-means algorithm can be described in 5 steps below. Another method developed by Lai et al. (2009) could be used if faster calculation is desired.

1) Make an initial guess of the k centroids;

2) Calculate the distance between every point to the cluster centroids. Euclidean distance in the parameter space is used in this study.

3) Assign each point to one specific group based on the minimum distances, which means a point belongs to one cluster having the nearest centroid from this point.

4) Calculate the new centroid for each group based on all members' coordinates

5) Repeat step 2–4 until all groups' membership become stable. One then obtains the final membership and the centroid of all clusters.

The results from the simple K-means method is shown in Fig.6a, while that from the SC algorithm is shown in Fig.6b. The latter is more applicable in this research for defining an exchange zone between the Kuroshio water and the shelf water of the ECS, likely resulting from the anisotropic T-S variance with it being more observable in the direction normal to the Kuroshio than the tangential.

3.1.2 Probability density function

To define an exchange zone quantitatively, we need to know to what degree a point belongs to each relevant The biggest advantage of the spectral clustering method rests on the probability density functions derived from this method, which can be used to calculate the degree of membership between each point and relevant clusters. Details of the steps are given below:

1) For any point $P_i\in\boldsymbol{P}$ (Fig.6a), the $dis_{i,kk}$($kk\in$ [1 k]) indicates the difference from the point P_i to

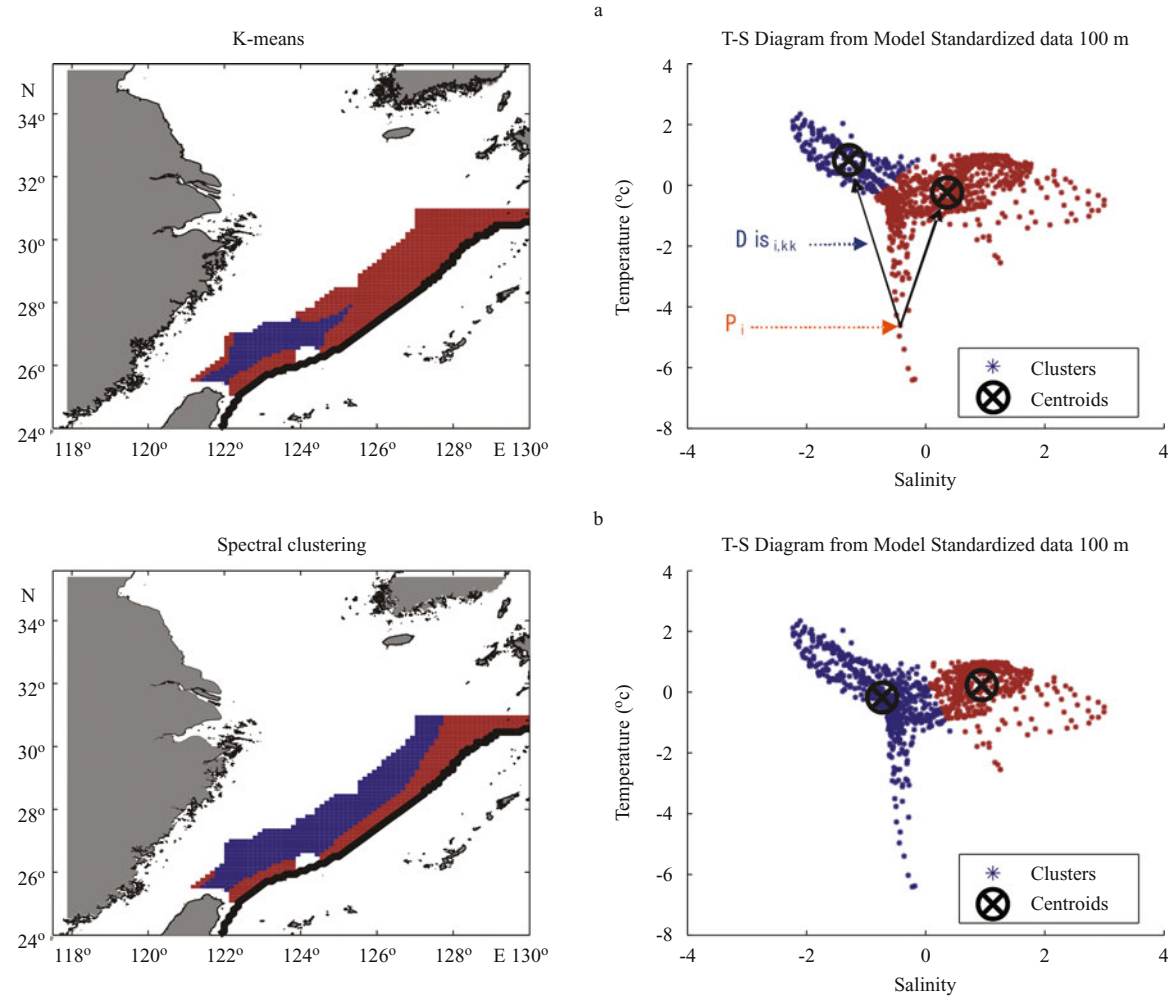

Fig.6 Examples of clustering analyses applied to the modeled T-S data (right) and its projection on the horizontal plain (left)
a. Result from the simple K-means algorithm; b. similar to (a) but using the spectral mixture method

the centroid of the group $m_{kk}(C_{kk})$. We use the Euclidean distance to compute $dis_{i,kk}$ here since the data has been standardized:

$$dis_{i,kk} = \|P_i - C_{kk}\| \tag{7}$$

2) Use $w_{i,kk}$, which is proportional to the reciprocal of $dis_{i,kk}$, to indicate a degree of membership for the point P_i associated with the cluster kk. If $\forall dis_{i,kk}(kk \in [1\ k]) \neq 0$,

$$w_{i,kk} = num_{kk} / dis_{i,kk} \tag{8}$$

Here, num_{kk} is the number of points $P_i \in m_{kk}$. If $\exists dis_{i,j}(j \in [1\ k]) = 0$,

$$w_{i,kk} = \begin{cases} 1 & (kk = j) \\ 0 & (kk \neq j) \end{cases} \tag{9}$$

3) Form the mixture distribution matrix $\boldsymbol{H}$. Let $w_{i \in P, kk \in M}$ be the weight of the degree of membership for P_i to be associated with M_{kk}. $H_{i,kk}$ is then the probability defined as

$$\boldsymbol{H}_{i,kk} = \frac{w_{i,kk}}{\sum_{j=1}^{k} w_{i,j}} \tag{10}$$

3.1.3 The exchange zone between clusters

To determine the exchange zones among the cluster set $\boldsymbol{T} = \{t_1, \ldots, t_v\}(t_i \text{-} m_j = \emptyset,\ 1 < v \leq k)$, set $\boldsymbol{R}_{m,n}$ and set $\boldsymbol{S}_{m,n}$ are introduced to calculate the limits between any two clusters of $\boldsymbol{t}_m$ and $\boldsymbol{t}_n$ in $\boldsymbol{T}$ $(m \neq n)$:

$$\begin{aligned} &\boldsymbol{R}_{m,n} \supseteq P_i \in \{\boldsymbol{t}_1 \cup \boldsymbol{t}_2 \ldots \cup \boldsymbol{t}_v\} \\ &\text{in which } |\boldsymbol{H}_{i,m} - \boldsymbol{H}_{i,n}| < \alpha_{m,n} (\alpha_{m,n} \in [0\ 1]) \end{aligned} \tag{11}$$

$$\begin{aligned} &\boldsymbol{S}_{m,n} \supseteq P_i \in \{\boldsymbol{t}_1 \cup \boldsymbol{t}_2 \ldots \cup \boldsymbol{t}_v\} \\ &\text{in which } |d_i| < \beta_{m,n} \times \min\left(\left|\overrightarrow{B}\right|, \left|\overrightarrow{E}\right|\right) \end{aligned} \tag{12}$$

Here, $\overrightarrow{B} = c_m \text{-} c_{mid}$, $\overrightarrow{E} = c_n \text{-} c_{mid}$, and $d_i = (\overrightarrow{A} \bullet \overrightarrow{B}) / |\overrightarrow{B}|$,

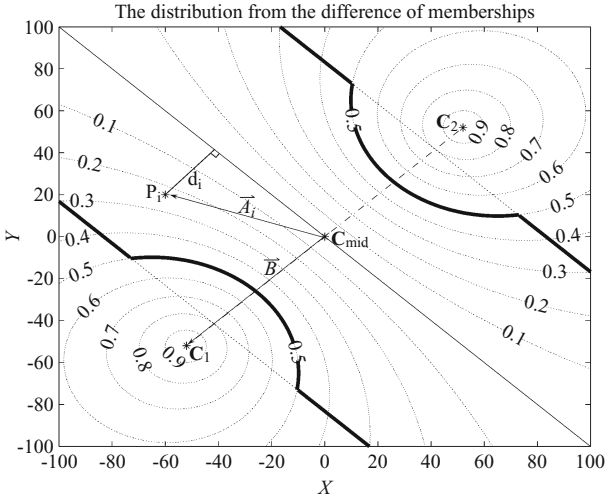

Fig.7 A mixing zone (the area between two thick lines) as determined by the SMM analysis in the case of v=2, α=0.5, β=0.8 and num_1= num_2. The isoclines show the value of R

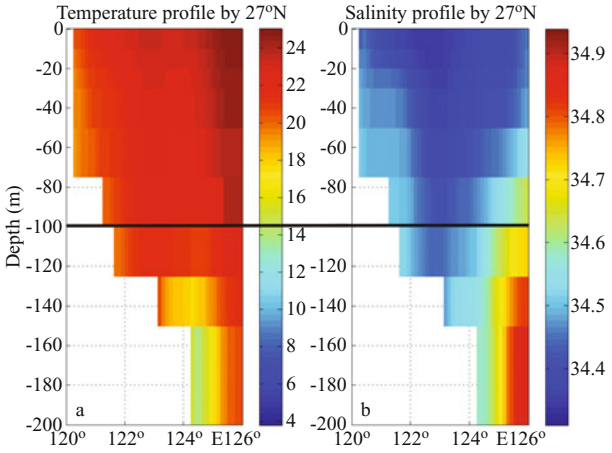

Fig.8 Climatological annual mean of the vertical section of temperature (a) and salinity (b) at 27°N

The black solid line indicates the depth of 100 meters

in which c_{mid}:=$(c_m \times num_n + c_n \times num_m)/(num_m + num_n)$ and $\overrightarrow{A}$ is a vector with the elements given by $\overrightarrow{A}_i = P_i - c_{mid}$. The graphical representation of these variables in a simple two cluster case is shown in Fig.7. The parameters α and β in Eq.11 and Eq.12 depend on the specific study of concern. In this study, α and β are finally set to 0.35 and 0.5 after many test trials. The exchange zone is then defined as

$$\boldsymbol{Z}_{m,n} = \boldsymbol{R}_{m,n} \cap \boldsymbol{S}_{m,n} \tag{13}$$

Here, $\cap\,(a_i)$:=$a_1 \cap a_2 \ldots \cap a_i$. $\boldsymbol{Z}_{m,n}$ includes all mixed points among $\boldsymbol{T}$ as $\boldsymbol{Z}$ (Fig.7):

$$\boldsymbol{Z} = \cap\left(\boldsymbol{Z}_{i,j},\ i \in [1\ v],\ j \in [1\ v],\ i \neq j\right) \tag{14}$$

3.2 Application of SMM to determine the exchange zone between the Kuroshio water and the shelf water in the ECS

The exchange zone between the Kuroshio water and the shelf water in the ECS is considered using the ROMS simulated temperature and salinity in this application. Based on the annual averaged temperature and salinity profile along the latitude at 27°N shown in Fig.8, the 100 m depth is chosen for the examination of this exchange zone since the distinctive appearance of the Kuroshio can be found in both the temperature and salinity at this level. To avoid the influence of the circulation in the Taiwan Strait and Tsushima Strait Current, we limit the latitudinal range to between 25 and 31°N. We also use the Kuroshio axis as the eastern boundary. We assume the core of the Kuroshio is bounded by the 0.4 m/s isotach in speed (Guan, 1980), and we use the maximum velocity point in the core as the position of the Kuroshio axis, which is similar to the definition of Andres et al. (2008). When compared with the temperature and salinity distributions with the World Ocean Atlas data (not shown), the temprature at 100 m is well simulated whereas the salinity is somewhat higher, but the patterns are similar.

Fig.9 shows the result of the SMM method with α=0.35 and β= 0.5, which appears to be a good combination of parameters for defining the exchange zone in our study. This method indicates a belt of exchange zone along the shelf break in the ECS. Compared to the belt in winter, the belt in summer is closer to the Kuroshio axis in the southwestern and mid segments, likely as a result of the summer monsoon driving the shelf water towards the open ocean. Another obvious difference is the presence of an exchange zone northwest of the Taiwan Island. This clearly shows the influence of the Kuroshio water on the ECS via the Taiwan Strait, but the influence diminishes in winter. The exchange zone is the widest in the northeastern segment and it has the most obvious seasonal swing with the zone clearly following the mean path of the Kuroshio in winter but veering towards the Korean Peninsula in summer. The strong seasonal variability of the exchange belt in segment 3 might be caused by the seasonal variability of Tsushima Current (Fig.1, Fig.3b). The T-S diagrams show wider ranges in the temperature and salinity in summer especially for the shelf water. Higher temperatures of the shelf water clearly result from seasonal warming,

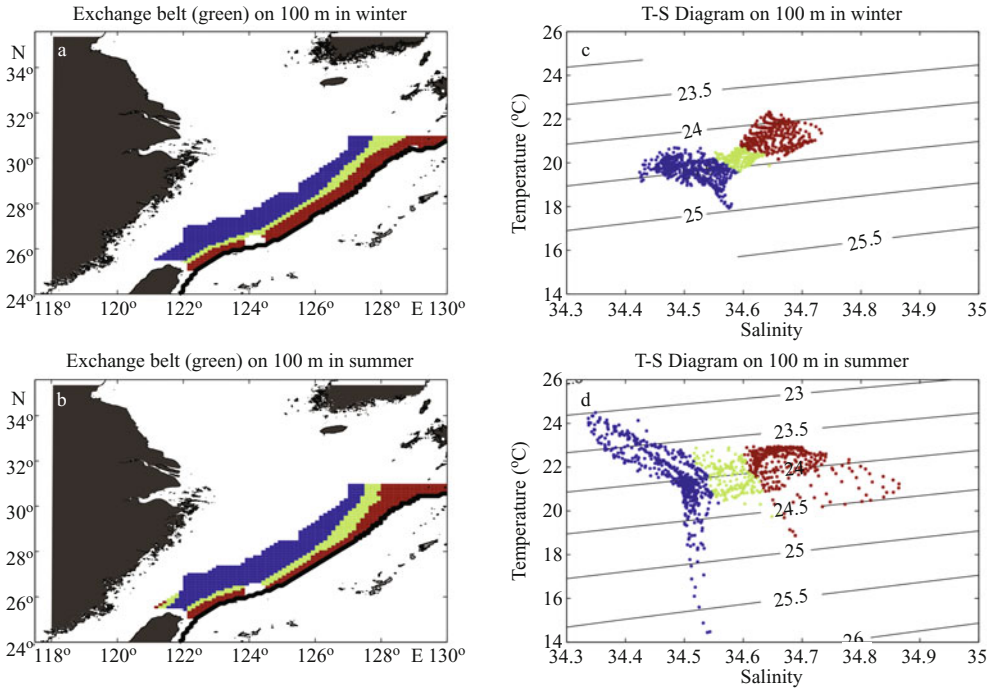

Fig.9 Analysis of the exchange zone at 100m in the ECS using SMM

Shown in (a) and (b) are distributions of the exchange zone in winter and summer, respectively. The corresponding TS scatter plots are shown in (c) and (d)

whereas the colder temperatures are located farther away from the Kuroshio.

The size of the exchange zone is then computed as the total area of the green shading, which is shown as the thick curve in Fig.10a. It varies seasonally with a minimum in January and often a second minimum in September. The biggest extent of the exchange zone occurs in April–July, with secondary peak often in November. We also analyzed the relationship between the exchange zone and the fluxes discussed above. There was a significantly negative correlation, -0.78, between the area of the exchange zone and the transport across the 200 m isobath along the shelf break in

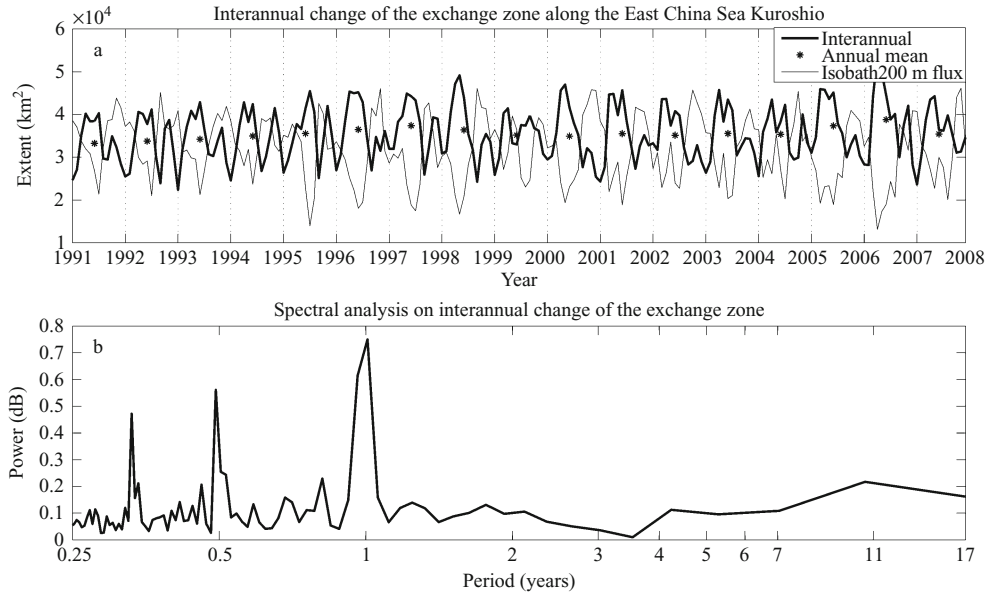

Fig.10 (a) Variability of the exchange zone area in the ECS (thick line) and the onshore flux across the 200-m isobath (f_{200}) by doing a coordinate transform (thin line): $f_{200} \times 10^4 + 2 \times 10^4$. Asterisks indicate the averaged value of each year from 1991 to 2008; (b) Spectrum of the exchange zone area shown in (a), which shows three peak periods at ~ 1 year, half year, and 3–4 months, respectively

the ECS (Fig.10). This significant correlation implies that the strong onshore volume flux tends to limit the water exchange between The Kuroshio and the shelf water in the ECS. A possible explanation is that they both relate to the variance of the Kuroshio position. When the Kuroshio becomes stronger, it forces more water onto the shelf hence larger fluxes across the 200 m isobath, but at the same time more water with significantly different temperature and salinity makes it harder to mix. Moreover, the total area of the exchange zone clearly shows the presence of the annual, semi-annual and intra-seasonal (3–4 months) variability, respectively. The lower limit of the confidence interval is about 0.23 for $P<5\%$ (95% significance), so all three frequencies are significant. The intra-seasonal variability is mostly caused by the westward Rossby Wave from the Pacific Ocean, but it is also possible from the interaction among the currents in the ECS.

4 DISCUSSION

The ROMS Pacific basin-wide simulation from 1991 to 2008 is used to depict the Kuroshio and the shelf currents in the ECS. The annual mean inflow (24°N) and outflow (130°E) of Kuroshio are estimated at 25.1 and 22.4 Sv, respectively, while the annual mean transport through the TS and the TUS are at 1.7 and 3.1 Sv. The difference between the pairs (24°N–130°E, or TUS – TS) is almost balanced by the net transport across the 200 m isobath onto the shelf. These annual mean values of transport as well as the seasonal transport through the TS and TUS are in good agreement with what have been reported in the published literature. The model also reveals an obvious seasonal variation in the onshore flux across the 200 m, which reaches the maximum in late fall and earlier winter and the minimum in summer. This seasonal variability comes partly from the enhanced Kuroshio intrusion northeast of Taiwan Island in response to the weakened northward Taiwan Current coming out the Taiwan Strait. Another interesting phenomenon hinted from the 18-year simulation is the decrease in amplitude of the seasonal variation of the transport at 24°N after the year of 2000. Processes that drive this phenomenon, most likely related to basin-wide long-term changes, warrant further investigation in the future.

The successful application of the SMM allows us define an exchange zone between the Kuroshio and the ECS shelf water. The SMM distinguishes itself from the traditional cluster analysis because it can compute the degree of association at the same time. The SMM is generally more general and efficient. The exchange zone as discussed in this paper follows the concept of Information Transition Zone (ITZ), which focuses on water property characteristics rather than the processes of material transport. Nevertheless, the exchange zone tends to correlate with the transport processes to some extent because the onshore transport brings the water mass to be mixed with the shelf water. On the other hand, the intrusion of the Kuroshio onto the shelf may squeeze the exchange zone, which appears as the inverse correlation between the exchange zone area and the net transport across the shelf break. In addition to the annual signal, significant peaks at periods of ~ 6 month and 3–4 months are found in the power spectrum from the time series of the exchange zone area, suggesting possible influences of the intra-seasonal signal from the Pacific on the exchanges between the Kuroshio and the ECS.

In this study the SMM is successfully applied to a simple case of only two water masses. It is worthwhile to point out that the SMM has potentially more extensive applications in water mass analyses and in studies of frontal processes. This method can be used to define the ITZs among any number of clusters by calculating the intercepts of multiple ITZs, each of which is defined between two given clusters as in this study. Fig.11 shows the intercept of two ITZs

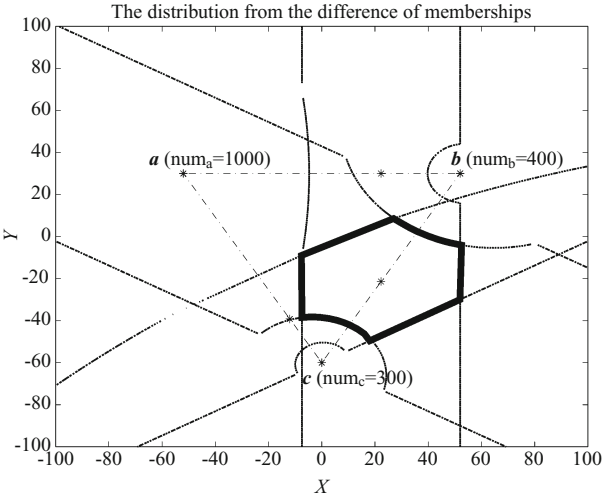

Fig.11 The zone amid thick polygon is the maximum limits for the case of $v=3$, $\alpha=0.5$, $\beta=1.0$

The number of points in each cluster (num_i, i represents either a, b, or c) is shown in the figure

among three clusters. Another issue is choosing num and two parameters, α and β. Methodologies to optimize these values need to be developed before extending the SMM to more general applications. The simple definition of num_{kk}, which stands for the number of object points in the cluster of m_{kk}, is used to represent the range of m_{kk} in this study. This definition is based on the assumption that the supposition of the points' distribution density of all clusters is uniform. Therefore, for problems with the distribution density varying from cluster to cluster, we suggest to replace num_{kk}/dd_{kk} with num_{kk} in Eq.8. The two parameters, α and β, can include not only the properties but also their gradients such as the information on thermocline and halocline. Doing so one can speed up the selection for the optimal α and β. Finally, the number of water masses (k) was prescribed in this study. Actually the optimal value of k can be determined automatically by analyzing the series of the eigenvalues from $\boldsymbol{L}$ (Eq.5). One idea is to sort the eigenvalues from the smallest to the largest and then find the k smallest eigenvalues whose sum is smaller than a ratio relevant to the sum of all eigenvalues. Improvements to SMM and other applications in oceanography are also being investigated in our laboratories, which shall be reported in future publications.

5 ACKNOWLEDGMENT

We thank Drs. Jianhui YUE and Jun CHEN at the Department of Electrical and Computer Engineering, the University of Maine. They checked the algorithms of the Spectral Clustering Method for its correctness. We also thank Dr. Xue'en CHEN in Ocean University of China; Dr. Lin MU in National Marine Data and Information Service and Dr. Xiuquan WAN in Texas A&M University for their helpful suggestions. Finally, we thank the three anonymous reviewers who provided constructive criticisms.

Reference

Andres M, Wimbush M, Park J H et al. 2008. Observations of Kuroshio flow variations in the East China Sea, *J. Geophys. Res.*, **113**(C05013), doi: 10.1029/2007JC004200.

Batchelor G K. 1967. An Introduction to Fluid Dynamic. Cambridge Univ. Press, London, U. K. p. 156-164.

Chai F, Liu G, Xue H et al. 2009. Seasonal and interannual variability of carbon cycle in South China Sea: A three-dimensional physical-biogeochemical modeling study. *J. Oceanogr.*, **65**: 703-720.

Chen C, Rou R, Paid S C et al. 1995. Exchange of water masses between the East-China-Sea and the Kuroshio off Northeastern Taiwan. *Cont. Shelf Res.*, **15**(1): 19-39.

Chen H, Yuan Y, Feng H. 2006. The multi-core structure of the main part of the Kuroshio at G-PN section in the East China Sea. *Chinese Sci. Bull.*, **51**(6): 738-746.

Chern C S, Wang J, Wang D P. 1990. The exchange of Kuroshio and East China Sea shelf water. *J. Geophys. Res.*, **95**(C9): 16 017-16 023.

Chuang W S, Liang W D. 1994. Seasonal variability of intrusion of the Kuroshio water across the continental shelf northeast of Taiwan. *J. Oceanogr.*, **50**(5): 531-542.

Clancy L J. 1975. Aerodynamics. Halsted Press, New York, U.S.A. p. 71-72.

Fukuoka J. 1957. A note on the westward intensification of ocean current. *Records of Oceanographic Works in Japan*, **1**: 7-8.

Guan B. 1980. Some results from the study of the variation of the Kuroshio in the East China Sea. In: the Kuroshio I V ed. Saikon Publ., Tokyo, Japan. p. 897-911.

Guo X, Hukuda H, Miyazawa Y et al. 2003. A triply nested ocean model for simulating the Kuroshio - roles of horizontal resolution on JEBAR. *J. Phys. Oceanogr.*, **33**(1): 146-169.

Guo X, Miyazawa Y, Yamagata T. 2006. The Kuroshio onshore intrusion along the shelf break of the East China Sea: The origin of the Tsushima Warm Current. *J. Phys. Oceanogr.*, **36**(12): 2 205-2 231.

Hu P, Hou Y, Le K et al. 2007. Study advances on the Kuroshio in the East China Sea and currents in the region east of Ryukyu islands. *Studia Marina Sinica*, **1**(00): 28-34. (in Chinese with English abstract)

Imasato N, Qiu B. 1987. An event in water exchange between continental-shelf and the Kuroshio off southern Japan - lagrangian tracking of a low-salinity water mass on the Kuroshio. *J. Phys. Oceanogr.*, **17**(7): 953-968.

Isobe A. 2008. Recent advances in ocean-circulation research on the Yellow Sea and East China Sea shelves. *J. Oceanogr.*, **64**: 569-584.

Isobe A, Beardsley R C. 2006. An estimate of the cross-frontal transport at the shelf break of the East China Sea with the Finite Volume Coastal Ocean Model. *J. Oceanogr.*, **111**(C0312), doi: 10.1029/2005JC003290.

James C, Wimbush M, Ichikawa H. 1999. Kuroshio meanders in the East China Sea. *J. Phys. Oceanogr.*, **29**(2): 259-272.

Jan S, Sheu D, Kuo H. 2006. Water mass and throughflow transport variability in the Taiwan Strait. *J. Geophys. Res.*, **111**(C12012), doi: 10.1029/2006JC003656.

Jia Y, Liu Q, Liu W. 2005. Primary study of the mechanism of eddy shedding from the Kuroshio bend in Luzon Strait. *J. Oceanogr.*, **61**(6): 1 017-1 027.

Jitendra M, Serge B, Thomas L et al. 2001. Contour and texture analysis for image segmentation. *Int. J. Comput. Vision*, **43**(1): 7-27.

Johns W E, Lee T, Zhang D et al. 2001. The Kuroshio east of Taiwan: Moored transport observations from the WOCE PCM-1 array. *J. Phys. Oceanogr.*, **31**(4): 1 031-1 053.

Kim K R, Cho Y K, Kang D J et al. 2005. The origin of the Tsushima Current based on oxygen isotope measurement. *Geophys. Res. Lett.*, **32**(3): L3602.

Lai J, Huang T J, Liaw Y C. 2009. A fast k-means clustering algorithm using cluster center displacement. *Pattern Recogn.*, **42**(11): 2 551-2 556.

Lan Y C, Lee M A, Liao C H et al. 2009. Copepod community structure of the winter frontal zone induced by the Kuroshio branch current and the

China coastal current in the Taiwan strait. *Journal of Marine Science and Technology-Taiwan*, **17**(1): 1-6.
Large W, McWilliams J C, Doney S C et al. 1994. Oceanic vertical mixing - A review and a model with a nonlocal boundary-layer parameterization. *Rev. Geophys.*, **32**(4): 363-403.
Lee J S, Matsuno T. 2007. Intrusion of Kuroshio water onto the continental shelf of the East China Sea. *J. Oceanogr.*, **63**(2): 309-325.
Li F, Xie J, Li Y. 2004. New methods of fitting the membership function of oceanic water masses. *Journal of Ocean University of China* (*English Edition*), **3**(1): 1-9.
Li G X, Han X, Yue S et al. 2006. Monthly variations of water masses in the East China Seas. *Cont. Shelf Res.*, **26**(16): 1 954-1 970.
Lin S, Hsieh I J, Huang K M et al. 2002. Influence of the Yangtze River and grain size on the spatial variations of heavy metals and organic carbon in the East China Sea continental shelf sediments. *Chem. Geol.*, **182**(2): 377-394.
Lin S F, Tang T Y, Jan S et al. 2005. Taiwan Strait current in winter. *Cont. Shelf Res.*, **25**(9): 1 023-1 042.
Liu G M, Chai F. 2009a. Seasonal and interannual variation of physical and biological processes during 1994–2001 in the Japan/East Sea: a three-dimensional physical-biogeochemical modeling study. *J. Marine Syst.*, **66**(2): 420-431.
Liu G M, Chai F. 2009b. Seasonal and interannual variability of primary and export production in South China Sea: A three-dimensional physical-biogeochemical model study. *J. Marine Sci.*, **78**(2): 265-277.
Luo B, Richard C W, Edwin R H et al. 2003. Spectral clustering of graphs. *Computer Analysis of Images and Patterns, Proceedings*, **2 756**: 540-548.
Ma C, Wu D X, Lin X P. 2009. Variability of surface velocity in the Kuroshio Current and adjacent waters derived from Argos drifter buoys and satellite altimeter data. *Chin. J. Oceanol. Limnol.*, **27**(2): 208-217.
Matsuno T, Lee J S, Yanao S. 2009. The Kuroshio exchange with the South and East China Seas. *Ocean Sci.*, **5**(3): 303-312.
Menschaert G, Tom T, Bart L et al. 2009. Spectral clustering in peptidomics studies helps to unravel modification profile of biologically active peptides and enhances peptide identification rate. *Proteomics*, **9**(18): 4 381-4 388.
Miller A R. 1950. A study of mixing processes over the edge of the continental shelf. *J. Mar. Res*, **9**(2): 145-160.
Mizuno K, White W B. 1983. Annual and interannual variability in the Kuroshio current system. *J. Phys. Oceanogr.*, **13**(10): 1 847-1 867.
Morimoto A, Kojima S, Jan S et al. 2009. Movement of the Kuroshio axis to the northeast shelf of Taiwan during typhoon events. *Estuar. Coast. Shelf S.*, **82**(3): 547-552.
Ng A Y, Jordan M I, Weiss Y. 2002. On spectral clustering: Analysis and an algorithm. *Advances in Neural Information Processing Systems*, **14**(1–2): 849-856.
Nitani H. 1972. Beginning of the Kuroshio. In: Kuroshio, Physical Aspects of the Japan Current. Univ. of Wash. Press, Seattle Wash., U.S.A. p. 129-164.
Shchepetkin A F, McWilliams J C. 1998. Quasi-monotone advection schemes based on explicit locally adaptive dissipation. *Mon. Weather Rev.*, **126**(6): 1 541-1 580.
Shchepetkin A F, McWilliams J C. 2003. A method for computing horizontal pressure-gradient force in an oceanic model with a nonaligned vertical coordinate. *J. Geophys. Res.*, **108**(C3), doi: 10.1029/2001JC001047.
Shchepetkin A F, McWilliams J C. 2005. The regional oceanic modeling system (ROMS): a split-explicit, free-surface, topography-following-coordinate oceanic model. *Ocean Modelling*, **9**(4): 347-404.
Shi J, Malik J. 2000. The 20th anniversary of the IEEE transactions on pattern analysis and machine intelligence. *Ieee T. Pattern Anal.*, **22**(1): 1-3.
Spall M A. 1995. Frontogenesis, subduction, and cross-front exchange at upper ocean fronts. *J. Geophys. Res.*, **100**(2): 2 543-2 558.
Stommel H. 1948. The westward intensification of wind-driven ocean currents. *Trans. Amer. Geophys. Union*, **29**(2): 202-206.
Su Y, Yu Z, Li F. 1983. Application of cluster analysis method for analyzing the water-masses in the shallow water area and the analysis of modified water masses in the Huanghai Sea and the East China Sea. *Chin. J. Oceanol. Limnol.*, **14**(1): 1-13.
Sverdrup H U, Johnson M W, Fleming R H. 1942. The Oceans, their Physics, Chemistry and General Biology. Pretince-Hall, New York, U.S.A. p. 16-64.
Takikawa T, Morimoto A, Onitsuka G et al. 2008. Characteristics of water mass under the surface mixed layer in Tsushima Straits and the southwestern Japan Sea in autumn. *J. Oceanogr.*, **64**(4): 585-594.
Tang T Y, Yang Y J. 1993. Low frequency current variability on the shelf break northeast of Taiwan. *J. Oceanogr.*, **49**(2): 193-210.
Teague W J, Jacobs G A, Ko D S et al. 2003. Connectivity of the Taiwan, Cheju, and Korea straits. *Cont. Shelf Res.*, **23**(1): 63-77.
Tong M R, Liu Z H, Sun C H et al. 2003. An analysis of data Quality Control Process of the ARGO Profiling Buoy. *Ocean Technology*, **22**(4): 79-84.
Ulrike L. 2007. A tutorial on spectral clustering. *Stat. Comput.*, **17**(4): 395-416.
Wang S L, Chen C, Hong G H et al. 2000. Carbon dioxide and related parameters in the East China Sea. *Cont. Shelf Res.*, **20**(4–5): 525-544.
Wei L, Liu Q, Jia Y. 2004. The Kuroshio transport east of Taiwan and the sea surface height anomaly from the Interior ocean. *Journal of Ocean University of China* (*Oceanic and Coastal Sea Research*), **3**(2): 135-140.
Wong G, Chao S Y, Li Y H et al. 2000. The Kuroshio edge exchange processes (KEEP) study - an introduction to hypotheses and highlights. *Cont. Shelf Res.*, **20**(4–5): 335-347.
Xiu P, Chai F, Shi L, Xue H et al. 2010. A census of eddy activities in the South China Sea during 1993–2007. *J. Geophys. Res.*, **115**(C03012), doi: 10.1029/2009JC005657.
Yanagi T., S. Takahashi. 1993. Seasonal variation of circulations in the East China Sea and the Yellow Sea. *J. Oceanogr.*, **49**: 503-520.
Yang J. 2007. An oceanic current against the wind: How does Taiwan island steer warm water into the East China Sea. *J. Phys. Oceanogr.*, **37**(10): 2 563-2 569.
Yuan Y, Liu Y, Su J. Variability of the Kuroshio in the East China Sea during El-Nino to La-Nina phenomenon of 1997 and 1998. *Chinese J. Geophys.*, **44**(2): 199-210.
Zhou H, Xu J, Guo P et al. 2006. A summary on studies of western boundary current system in the North Pacific Ocean. *J. Marine Sci.*, **24**(2): 49-59.
Zuo T, Wang R, Chen Y Q et al. 2006. Autumn net copepod abundance and assemblages in relation to water masses on the continental shelf of the Yellow Sea and East China Sea. *J. Marine Syst.*, **59**(1–2): 159-172.